Atomic Structure of Defects in GaN:Mg Grown with Ga Polarity

Z. Liliental-Weber, T. Tomaszewicz, D. Zakharov, J. Jasinski, and M. A. O'Keefe
Lawrence Berkeley National Laboratory, Berkeley, California 94720, USA
(Received 16 April 2004; published 10 November 2004)

The atomic structure of characteristic defects (Mg-rich hexagonal pyramids and truncated pyramids) in GaN:Mg thin films grown with Ga polarity was determined at atomic resolution by reconstruction of the scattered electron wave in a transmission electron microscope. Small cavities within the defects have inside walls covered by GaN of reverse polarity. We propose that lateral overgrowth of the cavities restores matrix polarity on the defect base. From matrix to defect, exchange of Ga and N sublattices leads to a 0.6 ± 0.2 Å displacement of Ga sublattices. We observe a $[1\underline{1}00]/3$ shift from matrix *AB* stacking to *BC* stacking for the entire pyramid. Electron energy loss spectroscopy detected changes in N edge and presence of oxygen on the defect walls. Our results explain commonly observed decrease of acceptor concentration in heavily doped GaN:Mg.

DOI: 10.1103/PhysRevLett.93.206102 PACS numbers: 68.35.Dv, 68.37.–d, 68.55.Ln

p-type doping of GaN still remains difficult and not well understood. The only efficient *p*-type dopant is Mg, but the free-hole concentration limit appears to be $\sim 2 \times 10^{18}$ cm^{-3} for Mg concentrations in the low 10^{19} cm^{-3} range, delaying further development of GaN-based devices. Increase of Mg concentration in metalorganic vapor-phase epitaxy films up to 1×10^{20} cm^{-3} leads to a decrease of the free-hole concentration (commonly interpreted as autocompensation due to increased formation of N vacancies or vacancy complexes with Mg [1]), and the occurrence of the so-called "blue band" in the photoluminescence spectra [2]. Transmission electron microscopy (TEM) studies of GaN:Mg show different types of Mg-rich structural defects that depend strongly on crystal growth polarity [3–6]. For bulk crystals grown with N polarity, planar defects (thin inversion domains) are formed on *c* planes creating an ordered structure [3]. Isolated three-dimensional Mg-rich hexagonal pyramids are formed in bulk platelet crystals and in metalorganic chemical vapor deposition GaN:Mg films grown with Ga polarity. Earlier studies show that the pyramids have bases on the (0001) plane and six sidewalls on $\{11\underline{2}3\}$ planes [4]. The direction from the tip of the pyramid to its base is along the Ga to N matrix bond direction [0002] [3–8]. Sidewalls appear inclined at 43° and 47°, respectively, to the base when observed in $[11\underline{2}0]$ [Figs. 1(a) and 1(c)] and $[1\underline{1}00]$ cross-section TEM micrographs [Figs. 1(b)]. Mg enhancement on the defect base and sidewalls was detected using energy dispersive x-ray spectrometry [3]. Trapezoidal defects, which we believe are truncated pyramids, are also present in these samples [Fig. 1(d)]. The two defects cannot be distinguished in plan-view configuration [Figs. 1(e) and 1(f)], suggesting a common origin and formation mechanism. For samples with the same [Mg] of 6×10^{19} cm^{-3}, the defect base size in MOCVD-grown thin films is (50–150 Å) and up to 1 order of magnitude larger in bulk crystals [4]. Our earlier studies [4–6], which were confirmed recently by Hautaakangas *et al.* [9], indicated the presence of holes inside the defects. However, there are also proposals in the literature that these defects might be Mg_3N_2 precipitates [10] or inversion domains imbedded in the matrix [7,11].

Since the increase of pyramidal defects coincides with the decrease of hole concentration [10] the knowledge of the defect's atomic structure appears to be of great importance. Using transmission electron microscopy (TEM) to produce the complex two-dimensional electron wave at the specimen exit surface (the ESW), we have obtained the first atomic-scale information about these defects in specimens where they were not superimposed with the matrix (mostly bulk crystals). We then compared results obtained on smaller defects (mostly in MOCVD-grown thin films). The phase advance of the ESW phase has peaks at the atom positions with heights proportional to the projected potential of the column of atoms underlying the peaks and thus to the number of atoms making up the column (and to their atomic number—heavier atoms produce more phase advance). For monoatomic columns, one can distinguish between different elements

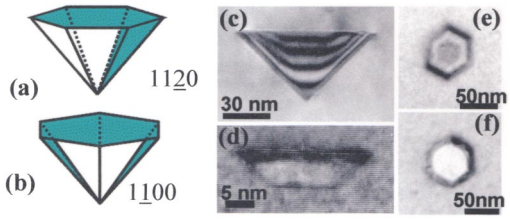

FIG. 1 (color online). Schematic drawings of defects formed in GaN:Mg in the two crystallographic directions 11$\underline{2}$0 (a) and 1$\underline{1}$00 (b); (c) TEM image in which a pyramid is seen as a triangular defect and (d) as a trapezoid (a truncated pyramid). These defects (as shown) are always arranged with Ga polarity; i.e., the long bond direction along the *c* axis from the triangle tip to the base (or shorter base to longer base in a trapezoid) is from Ga to N; (e),(f) plan-view images of the same defects reveal the different sectioning.

and estimate the number of atoms in the column. We reconstructed the specimen ESW from focal series of high-resolution TEM images [12], and used it to determine defect structure and growth polarity by distinguishing the particular atoms contributing to the image.

Increasing specimen thickness increases the advance of the ESW phase, driving the complex vector at the atom position in a counterclockwise Argand-plane trajectory. The phase advance at an atom column position is always greater for Ga than for N at the same thickness (same number of atoms), allowing identification of Ga and N columns [Figs. 2(a) and 2(b)] and determination of crystal thickness and polarity. Although the ESW phase repeats at much greater thickness, best reconstructions are obtained at small sample thickness. Color coding [Fig. 2(c)] was applied to present the map of ESW phase advance relative to the vacuum wave [13,14]. Application of this method to analyze a stacking fault in GaN imaged in [11$\underline{2}$0] projection confirmed the nature of this defect (previously obtained from classical TEM) and the matrix Ga growth polarity (obtained earlier from convergent-beam electron diffraction studies). Color coding gave the correct positions of Ga and N atoms, allowing us to see *AB* atom arrangement below the fault and *BC* above it.

Following these encouraging results, the same method was applied to pyramidal defects in GaN:Mg. A schematic drawing [Fig. 3(a)] shows the site of an experimental image of part of a pyramidal defect [Fig. 3(b)] containing a hole (amorphous area in the left corner). It is clear that the defect is not a simple void. To suit the 0.8 Å resolution of our 300 kV modified CM30 microscope [15], most studies were performed in [11$\underline{2}$0] projection with the defect side walls not in end-on configuration. End-on [1$\underline{1}$00] studies show only Ga positions (with the more advanced phase) since the projected 0.6 Å distance between Ga and N is beyond the microscope's resolution.

To obtain a reasonable statistic, ESW phase advances (each reconstructed from 20 images) were obtained in [11$\underline{2}$0] projection for different areas of several pyramids. Matrix ESW phase advances above the pyramid base [Fig. 3(c)], below the pyramid tip [Fig. 3(e)], and on the pyramid side [Fig. 3(g)] show atomic column positions with two distinct intensity spots at Ga and N atom positions, confirming the expected Ga polarity with the "*AB*" atomic stacking that is characteristic for hexagonal structure. The ESW phase advance inside the pyramid, on the walls including the pyramid tip [Fig. 3(d)], shows N growth polarity, an inversion compared to the matrix. In addition, "*AB*" stacking in the matrix changes to "*BC*" stacking within the pyramid, giving an $a/3$ shift [Figs. 3(d) and 3(e)]. This atomic stacking arrangement holds through the entire pyramid. Change back to the matrix "*AB*" stacking takes place at the pyramid base [Fig. 3(c)].

ESW phase images along a *c* plane [Figs. 3(f) and 3(g)] show a change of matrix Ga columns to pyramid N columns, giving a measured 0.6 ± 0.2 Å displacement (along *c* axis) on the pyramid side between Ga positions in the matrix and the pyramid (at some distance from the defect sidewall to avoid overlapping with the matrix). The same0.6 ± 0.2 Å results were obtained from small pyramids present in MOCVD thin foils measured in [1$\underline{1}$00] projection where side walls are in edge-on configuration.

Measurements show that *c*-plane spacing slightly above the pyramid base is 0.2 Å greater than the matrix value far from the pyramid and increases monotonically to become 0.6 Å greater at the base. Expansion of *c*-plane spacing, and less ESW phase advance observed at the defect base, suggest decoration by Mg of several planes close to the base. Shifts of 0.6 Å on the defect wall are consistent with increased *c*-plane spacing on the defect base, and show that polarity change close to the defect tip due to Mg presence would require at least 0.6 Å shift on the defect base.

Electron energy loss spectroscopy (EELS) from the central parts of the pyramidal defect were identical to this observed in the matrix [Fig. 4(a)]. These results would rule out the possibility of Mg_2N_3 phase formation, contradicting earlier results [10]. However, when the electron beam was placed on the pyramidal defect base or on defect walls a drastic change of shape occurred in the NK_α edge [Figs. 4(b) and 4(c)]. The presence of oxygen was also observed [Fig. 4(d)].

Several models have been proposed for inversion domains in GaN:Mg. Our two earlier models, proposed for flat N-polar to Ga-polar domain interfaces in crystals grown with N polarity, introduced a shift of $[1\underline{1}00]/3 + c/2$ [4]. In our samples grown with Ga polarity, similar $[1\underline{1}00]/3$ shifts are observed with change from *AB* stacking in the matrix to *BC* within the entire pyramid. Northrup's "abcab" model [16] gives the lowest energy but considers only one layer rich in Mg, on the "C" stacking position, and is not consistent with our experimental observation. Romano [17] suggests the Ga matrix sublattice on *c* plane continues across the pyramid side, while Vennegues [11] considers the N sublattice to continue, as similarly proposed by Northrup [16]. The latest model would require 1.3 Å shift between the Ga sublattices outside and inside the pyramid. Our atomic resolution with ESW phase provides for the first time a detailed atomic arrangement at the pyramidal defect, and shows how Ga and N positions on the *c*-plane interchange from matrix to defect to produce a shift of 0.6 ± 0.2 Å between Ga sublattices.

We believe that pyramids (and truncated pyramids) start to grow from the Mg-rich clusters (often observed with less ESW phase advance in both bulk and MOCVD-grown samples) observed in the matrix close to the pyramidal tips. Depending on cluster size either pyramids or truncated pyramids are formed.

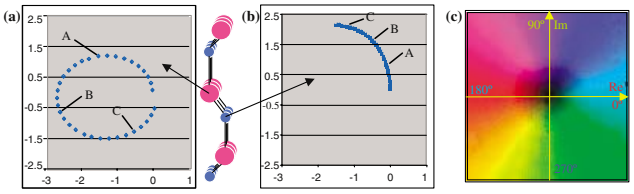

FIG. 2 (color). Argand plot of the ESW from a multislice-simulated GaN sample, showing trajectories of complex ESW values for Ga (a) and N (b). In both (a) and (b) different number of simulated atoms in the column are indicated; *A*, *B*, and *C* correspond to 10, 20, and 30 atoms, respectively. This shows that phase advances faster for Ga then N atoms. An inset shows atomic arrangement in our sample; (c) shows the colors used to code ESW images for phase advances.

The 43° and 47° angles between pyramid sides and its base observed in [11$\underline{2}$0] and [1$\underline{1}$00], respectively, confirm the side defect plane to be (11$\underline{2}$3). One can notice that this plane is almost equally occupied by Ga and N and Mg can be easily attracted by both these atoms forming double a Mg-rich layer on the defect walls. In this way decoration by Mg on the side walls can happen very quickly, especially when Mg-rich clusters are formed, leading to a local polarity change and formation of a defect. However, growth of GaN with reverse polarity at the defect would be much slower [18] than matrix growth, leading to meniscus formation, and later a hole. Pyramid growth would terminate with a minute lack of Mg on the defect walls allowing fast lateral overgrowth along *c* planes. This lateral overgrowth would explain formation of an abrupt defect base as observed experimentally. Further rearrangement of Mg, Ga, and N would take place inside the pyramid below the base. Since Mg always floats toward the surface, it is therefore not surprising to observe *c* planes rich in Mg close to the defect base, giving less ESW phase advance and *c*-plane expansion. In addition, Mg oxidation can take place if oxygen is available in the growth chamber, due to high Mg to O affinity, and compounds such as MgO or Mg-N-O can be formed on all defect walls, explaining the change of shape of the NK_α edge and oxygen presence detected by EELS. It is also possible that attraction of Mg to oxygen insures faster growth of the pyramid as observed in bulk crystals, where oxygen concentration is much higher, compared to these grown by MOCVD [6], and are hardly reported in molecular-beam epitaxy grown layers.

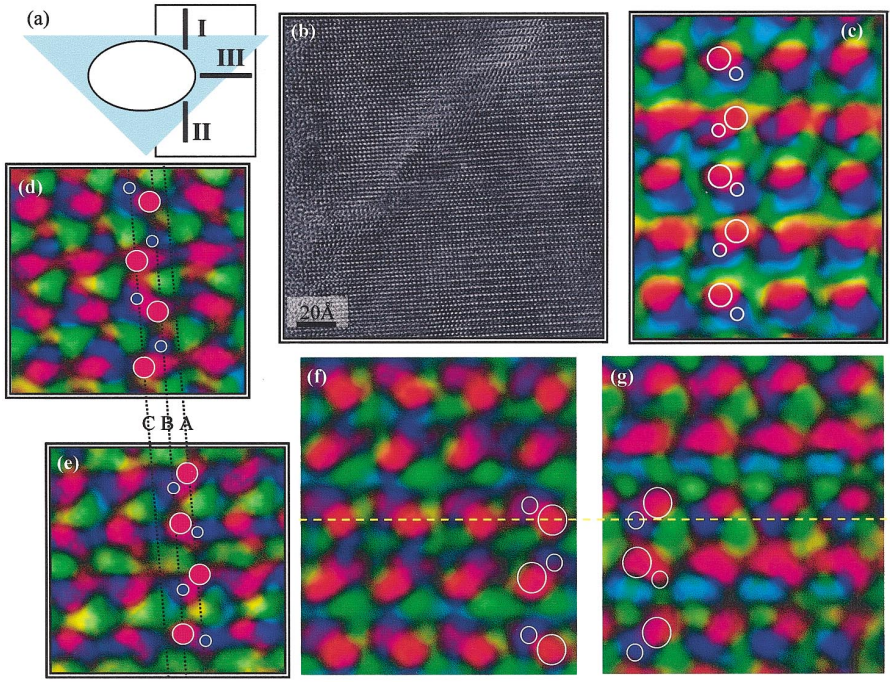

FIG. 3 (color). (a) Schematic of a pyramidal defect with a hole inside the defect; lines in the box with numbers I, II, and III indicate areas from which experimental images were taken. (b) Cross-section TEM experimental image from part of the pyramid close to the pyramid tip—schematically shown as an inset box in (a), a hole is visible inside the pyramid (amorphous contrast) in the left lower corner of the micrograph; (c)–(g) Color images of the phase advance from the experimentally reconstructed ESW: (c) the matrix above the defect base area I in (a) confirms Ga growth polarity; (d),(e) the area II indicated in (a), with (d) inside the pyramid close to the defect tip and (e) from the matrix below the defect. These two micrographs are lined up along *c* axis and show "*AB*" atomic stacking within the matrix (e) and "BC" within the defect (d). Note change of polarity in (d) compared to (e); (f),(g) arrangement of atomic column positions along *c* plane within and outside the defect indicated by III in (a); (f) inside the defect and (g) in the matrix outside the defect. Note the exchange of Ga and N sublattices inside and outside the defect (indicated by dotted line).

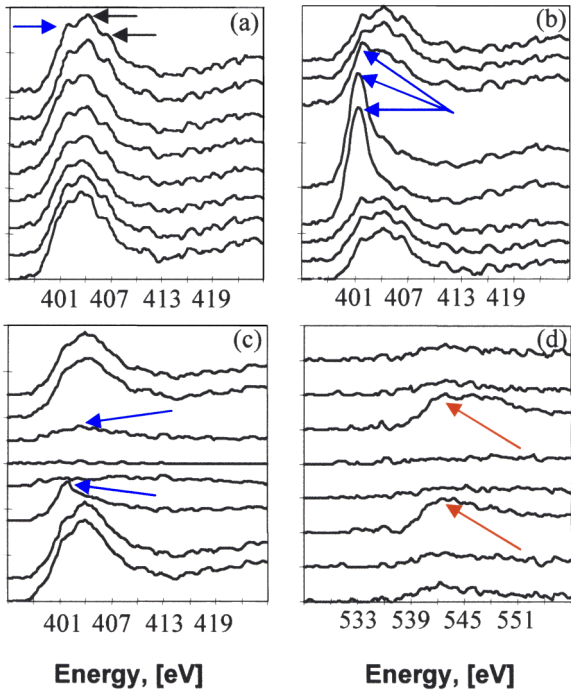

FIG. 4 (color online). Electron (EELS) from defects and the surrounding matrix; (a) the NK_α edge has three maxima (arrows). Eight spectra are shown; the two lower lines and the two upper lines are from the matrix and four center lines are from the crystalline part of the triangular defect where reverse polarity was found; (b) The NK_α edge of the triangular defect with its side within the TEM thin foil (three center lines). Note an increase of intensity of the left maxima (arrows) compared with the matrix (three lower and two upper lines); (c) The NK_α edge from the trapezoidal defect [with a hole inside and two bases as in Fig. 1(d)] shows an enhanced left peak (arrows) when the electron beam touches the top and bottom bases (third lines from the top and bottom) compared with the matrix (two lower and two upper lines); flattening of the peaks is seen when the electron beam hits the hole (two center lines); (d) The O$K_\alpha$edge from the same defect taken simultaneously with the spectra shown in (c). Note an increase of oxygen peak (arrows) when the electron beam intersects the upper and the lower bases of the defect.

Using exit wave phase imaging in a modified TEM, we showed that two types of defects in bulk GaN:Mg crystals are hexagonal pyramids and truncated pyramids with six inclined walls and a base formed on the GaN *c* plane. We believe these defects grow from Mg-rich clusters accumulating on *c* planes. Both defects contain holes in their centers, but their walls are covered by a substantial thickness of GaN grown with opposite polarity to the matrix. This inversion and presence of oxygen detected by EELS on the defect bases and their walls would lead to Mg compensation and a decrease of possible Mg_{Ga} acceptor density with an increase of Mg concentration, since the number of defects and their size increases in such samples. This study would explain earlier observations [1] showing a decrease of free-hole concentration with an increase of Mg. Our atomic resolution results show that Mg_2N_3 is not formed inside the defect as suggested earlier [10], but an exchange of the Ga and N sublattices outside and inside the defects leads to a displacement of 0.6 ± 0.2 Å between the Ga sublattices in these two areas. Our results show that change of polarity starts from the defect tip and propagates to the base, terminating by lateral overgrowth of the cavities formed within the defect to ensure a return to matrix polarity on the defect base.

This work was supported by the U.S. Department of Energy under Contract No. DE-AC03-76SF00098. Use of the OÅM facility at the National Center for Electron Microscopy at the LBNL is greatly appreciated.

[1] U. Kaufman, P. Schlotter, H. Obloch, K. Kohler, and M. Maier, Phys. Rev. B **62**, 10867 (2002).
[2] S. Nakamura and G. Fasol, *The Blue Laser Diode* (Springer-Verlag, Berlin, 1997).
[3] Z.Liliental-Weber *et al.*, Phys. Rev. Lett. **82**, 2370 (1999).
[4] Z. Liliental-Weber, M. Benamara, W. Swider, J. Washburn, I. Grzegory, S. Porowski, R. D. Dupuis, and C. J. Eiting, Physica (Amsterdam) **273B–264B**, 124 (1999).
[5] Z. Liliental-Weber, M. Benamara, J. Washburn, I. Grzegory, S. Porowski, D. J. H. Lambert, C. J. Eiting, and R. D. Dupuis, Appl. Phys. Lett. **75**, 4159 (1999).
[6] Z. Liliental-Weber, J. Jasinski, M. Benamara, I. Grzegory, S. Porowski, D. J. H. Lambert, C. J. Eiting, and R. D. Dupuis, Phys. Status Solidi (b) **228**, 345 (2001).
[7] P. Vennegues, M. Benaissa, S. Dalmaso, M. Leroux, E. Feltin, P. De Mierry, B. Beaumont, B. Damilano, N. Grandjean, and P. Gibbar, Mater. Sci. Eng. B **93**, 224 (2002).
[8] R. Kroger, S. Figge, T. Bottcher, P. L. Ryder, and D. Hommel, Mater. Res. Soc. Symp. Proc. **693**, 615 (2002).
[9] S. Hautaakangas, J. Oila, M. Alatalo, K. Saarinen, L. Liszkay, D. Seghier, and H. P. Gislason, Phys. Rev. Lett. **90**, 137402 (2003).
[10] M. Hansen, L. F. Chen, J. S. Speck, and S. P. DenBaars, Phys. Status Solidi (b) **228**, 353 (2001).
[11] P. Vennegues, M. Leroux, S. Dalmasso, M. Benaissa *et al.*, Phys. Rev. B **68**, 235214 (2003).
[12] A. Thust, W. M. J. Coene, M. Op De Beeck, and D. Van Dyck, Ultramicroscopy **64**, 211 (1996).
[13] D. Van Dyck and M. Op De Beeck, Ultramicroscopy **64**, 99 (1996).
[14] W. Sinkler and L. D. Marks, Ultramicroscopy **75**, 251 (1999).
[15] M. A. O'Keefe, E. C. Nelson, Y. C. Wang, and A. Thust, Philos. Mag. B **81**, 1861 (2001).
[16] J. E. Northrup, Appl. Phys. Lett. **82**, 2278 (2003).
[17] L. T. Romano, J. E. Northrup, A. J. Ptak, and T. H. Myears, Appl. Phys. Lett. **77**, 2479 (2000).
[18] Z. Liliental-Weber, Y. Chen, S. Ruvimov, and J. Washburn, Phys. Rev. Lett. **79**, 2835 (1997).